



ISTITUTO NAZIONALE DI RICERCA METROLOGICA Repository Istituzionale

Solid silica nanoparticles as carriers of fluorescent squaraine dyes in aqueous media:
Toward a molecular engineering approach

This is the author's submitted version of the contribution published as:

Original

Solid silica nanoparticles as carriers of fluorescent squaraine dyes in aqueous media: Toward a molecular engineering approach / Alberto, G.; Barbero, N.; Divieto, C.; Rebba, E.; Sassi, M. P.; Viscardi, G.; Martra, G. - In: COLLOIDS AND SURFACES. A, PHYSICOCHEMICAL AND ENGINEERING ASPECTS. - ISSN 0927-7757. - 568:(2019), pp. 123-130. [10.1016/j.colsurfa.2019.01.052]

Availability:

This version is available at: 11696/59983 since: 2021-03-04T17:15:34Z

Publisher:

Elsevier

Published

DOI:10.1016/j.colsurfa.2019.01.052

Terms of use:

This article is made available under terms and conditions as specified in the corresponding bibliographic description in the repository

Publisher copyright

(Article begins on next page)

Solid silica nanoparticles as carriers of fluorescent squaraine dyes in aqueous media: toward a molecular engineering approach

3

4 Gabriele Alberto^{a,*}, Nadia Barbero^{a,*}, Carla Divieto^b, Erica Rebba^a, Maria Paola Sassi^b, Guido
5 Viscardi^a, Gianmario Martra^a

6

7 ^a *Department of Chemistry, NIS Interdepartmental and INSTM Reference Centre, University of*
8 *Torino, Via Pietro Giuria 7, 10125 Torino, Italy*

9 ^b *Italian National Insititute for Metrological Research INRIM, Strada delle Cacce 91, 10135*
10 *Torino, Italy*

11

12 *E-mail addresses:* gabriele.aberto@unito.it, nadia.barbero@unito.it , c.divieto@inrim.it,
13 erica.rebba@unito.it, m.sassi@inrim.it, guido.viscardi@unito.it, gianmario.martra@unito.it

14 **Corresponding authors*

15

16 *Keywords:* squaraines in water; hybrid dye-silica solid nanoparticles; fluorescence; tissue optical
17 window.

18

19 *Highlights*

- 20 • Water insoluble and soluble squaraine dyes were encapsulated inside solid silica nanoparticles
21 50±2 nm in size by exploiting the reverse microemulsion method
- 22 • Hybrid dye-SiO₂ nanoparticles with photoluminescent intensity per dye molecule similar to that
23 of squaraines in organic solvent were prepared
- 24 • The hydrophilicity of squaraine-3-aminopropyltriethoxysilane (APTS) adducts is a key
25 parameters ruling the dispersion of the fluorophors within the nascent silica matrix
- 26 • The administration of the squaraine-APTS adducts together with the co-surfactant plays also a
27 relevant role

28

29 **Abstract**

30 **Hypothesis.** The relative hydrophilicity of dye-3-aminopropyltriethoxysilane (APTS) adducts and
31 tetraethylorthosilicate (TEOS) plays a key role in determining the distribution of fluorophores when
32 preparing hybrid dye-SiO₂ fluorescent nanoparticles, intended to be used in aqueous media. Here,
33 this hypothesis is applied to the case of high quantum-yield squaraine dyes, otherwise insoluble in
34 such media, and suffering a severe decrease of quantum yield if derivatised with polar groups and
35 dissolved in water.

36

37 **Experiments.** Hybrid squaraine-SiO₂ nanoparticles extremely homogeneous in size (50±2 nm) were
38 prepare by using the reverse microemulsion technique. Three different squaraine dyes were used and
39 the photophysical behavior of the prepared samples were qualitatively and quantitatively studied, by
40 steady state and time-resolved photoluminescence, in order to establish structure-property
41 relationships useful for the optimization of the preparation method.

42

43 **Findings.** Hybrid squaraine-SiO₂ nanoparticles with fluorescent intensity per dye molecule similar
44 to that of parent squaraines in organic solvent were successfully prepared. The role of the
45 hydrophilicity of the dye-APTS adduct in ruling the dispersion of such adduct in the nascent silica
46 matrix was confirmed, and the possibility to improve the tuning of the process by properly
47 administration of the adduct with the co-surfactant was demonstrated.

48

49

50

51

52

53 1. Introduction

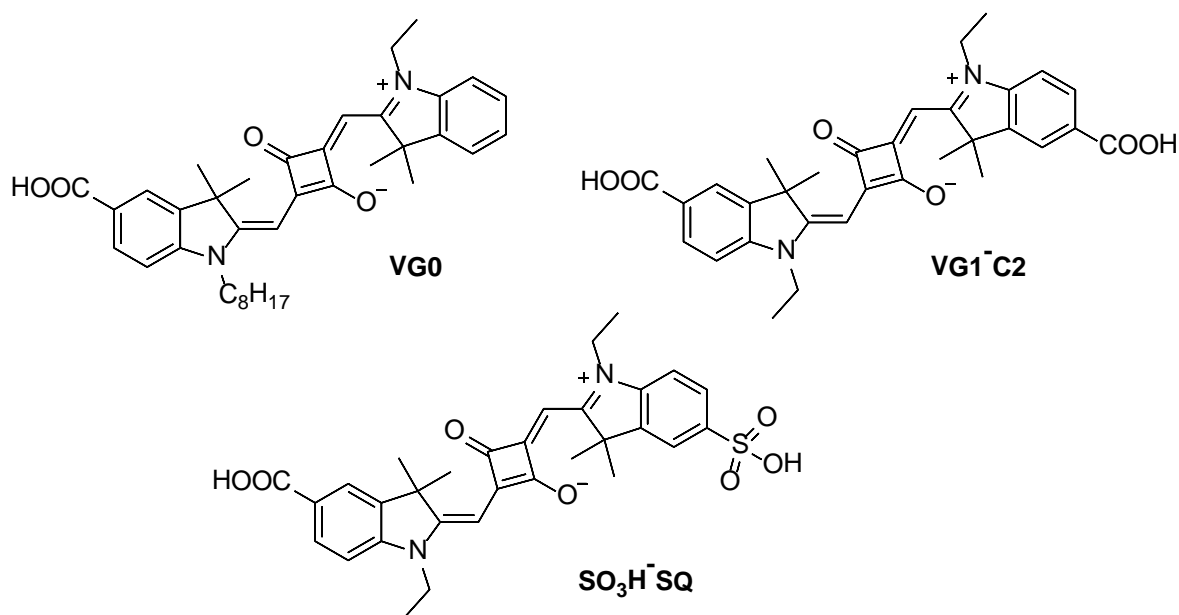
54

55 Organic dyes with absorption in the optical tissue window from 600 to 850 nm (where the self-
56 fluorescence of biological molecules is negligible) have emerged as a promising tool for bioanalytical
57 or biologically related applications and for *in vivo* fluorescence imaging. Polymethine dyes[1], such
58 as cyanines and squaraines, offer numerous advantages such as their easiness in designing new
59 molecules with the desired photochemical properties simply by elongating the central bridge and/or
60 tuning the lateral functional groups[3]. In this manner, dyes with absorption and emission spectra
61 properly located in the optical tissue window are obtained[4]. Cyanines and squaraines have both
62 their own pros and cons, however squaraines, resulting from the dicondensation between squaric acid
63 and electron rich molecules, are typically characterized by a quantum yield and a photostability
64 significantly higher than those found for cyanines[5]. Unfortunately, squaraines are poorly soluble in
65 aqueous media, and the consequent easy formation of non-fluorescent aggregates heavily limited their
66 adoption as fluorescent markers for biological applications. Moreover, the usual strategy used in
67 organic chemistry targeting, i.e. the introduction of a group ionizable in water, such as a sulfonic
68 moiety, is detrimental, because once dissolved in water, such derivatized squaraine dyes show a very
69 low quantum yield with respect to pristine fluorophores dissolved in less polar media[6]. In order to
70 overcome these problems, the incorporation of these hydrophobic dyes in carriers appeared to be a
71 mandatory step for their dispersion in physiological conditions. As far as molecular carriers are
72 concerned, a proposed approach is the encapsulation of the dye inside a permanently interlocked
73 rotaxane molecule, also increasing the resistance to chemical and photochemical degradation[7], or
74 in micelles[8]. Moreover, SQ-based self-assembly in hydrophobic phospholipid bilayers of liposomes
75 were successfully used for *in vivo* imaging[9]. In the domain of inorganic carriers, a possibility is the
76 intercalation of photoactive compounds into hydrotalcite (layered double hydroxides; LDH)[10], or
77 they can be loaded inside amorphous silica nanoparticles, depending on the specific application.
78 When multifunctional nanoplatfroms are pursued, the materials of interest are mesoporous silica

nanoparticles, used as such, for instance for photodynamic therapy[11], or wrapped with graphene oxide sheets, to protect the squaric ring from possible nucleophilic attack of molecular components of *in-vitro* and *in-vivo* biological media[12]. When imaging is the intended application, a relevant nanocarrier is constituted by solid non-porous silica nanoparticles (NPs), highly protecting encapsulated dye molecules[13–15]. Hybrid dye doped solid silica NPs can be prepared by hydrolysis and polycondensation of a silicon alkoxide, such as tetraethylorthosilicate (TEOS), and fluorophores derivatized with an alkoxy silane moiety, allowing the encapsulation of dye molecules in the nascent silica matrix. The process can be carried out in homogeneous solution[16], i.e. exploiting the so-called Stöber method, or in reverse microemulsion[17]. In both cases, the condensation reaction among molecular precursors of silica typically occurs by addition of a basic agent, and this can prevent the production of silica NPs hybridized with dyes as penta/hepta-methine cyanines, which do not resist a high pH. Conversely, squaraines do not suffer this limitation, and then appear as relevant organic dyes to be vehiculated in aqueous media by entrapment in silica NPs. Despite the complexity of the synthesis procedure, the microemulsion method can be preferred to the Stöber one, owing to the possibility to obtain particles with a very narrow size distribution, thus simplifying at least one aspect of the complex combination of parameters affecting the behavior of nanomaterials in biological media. Moreover, previous research works devoted to the encapsulation of three methine cyanines[18,19] allowed to highlight that the dispersion of these visible dye molecules throughout the nascent silica matrix is ruled by the relative hydrophilicity of TEOS and the dye-APTS adduct, kinetically competing for the water pool inside reverse micelles[13]. Avoiding aggregation of dyes within the nanocarrier is mandatory to preserve photoemission performances. To the best of our knowledge, no examples of squaraine dyes encapsulated in amorphous silica NPs have been reported so far.

This was the basis of the present work, devoted to the elucidation of molecular aspects and preparation procedures relevant for the production of photoluminescent hybrid squaraines-SiO₂NPs. To this aim, three squaraine dyes with different chemical structures and degree of hydrophilicity (figure 1) were

105 used to synthesize silica NPs by the reverse microemulsion method. Each sample was characterized
106 in terms of size and morphology by electronic transmission microscopy and their photophysical
107 properties were investigated by UV-Vis absorption and steady-state/time-resolved photoemission
108 spectroscopy in order to define structure-property relationships useful for the optimization of the
109 photoemission performances.



111
112
113 **Figure 1.** Structures of VG0, VG1-C2 and SO₃H-SQ.

114 115 116 **2. Experimental details**

117 118 **2.1 Syntheses: chemicals and procedures**

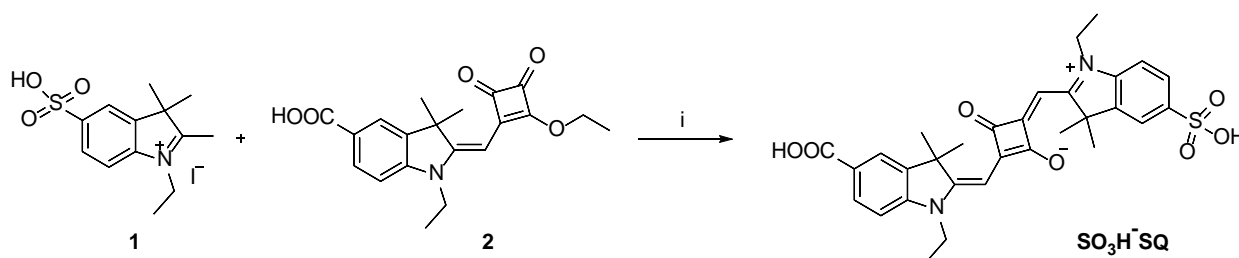
119 All reagents and solvents, of a highly pure grade, were purchased from Sigma Aldrich, Fluka, Merck
120 or Riedel de Haen and were used without any further purification.

2.1.1 Synthesis of squaraines

VG0 and **VG1-C2** were prepared as previously described[3]. For the synthesis of **SO₃H-SQ** a modified procedure as reported in the literature [3,20] was followed. An equimolar mixture (0.84 mmol) of compound **1** and **2** (scheme 1) were introduced into a 20 ml microwave reaction vial with toluene and butanol (18 ml, 1:1), sealed with a crimp cap and heated in the microwave system (single-mode Biotage Initiator 2.5) at 160°C for 25 min. The green precipitate which is formed is washed with diethyl ether and further purified by a semi-preparative HPLC system (by Shimadzu, equipped with SCL 10Avp, SPD 10Avp, a LC8A pump and a Phenomenex column Synergi Fusion-RP 4 μ , 150x21.20 mm) using an isocratic flow of methanol with formic acid (1%, v/v) to obtain **SO₃H-SQ** (105 mg, yield = 22%) as a green powder.

¹H NMR (200MHz, D₂O), δ : 8.01-7.72 (m, 6H), 7.15 (s, 1H), 6.91 (s, 1H), 4.42 (m, 2H), 3.79 (m, 2H), 1.47 (s, 12H), 1.14 (s, 6H).

MS (ESI) [M-H]⁻ 575.60



Scheme 1. Synthesis of **SO₃H-SQ**. Experimental conditions: (i) toluene/butanol (1:1), MW, 25 min, 160°C.

2.1.2 Synthesis of squaraine-silane derivatives

The *N*-Hydroxysuccinimide (NHS) active esters of the two non-symmetrical squaraines **VG0** and **SO₃H-SQ** were synthesized by reacting 0.02 mmol of each fluorophore with NHS (0.08 mmol) and *N,N'*-Dicyclohexylcarbodiimide (DCC, 0.08mmol) in dimethylformamide (DMF, 2.0 ml) and stirring

for 4h at 80°C; in the case of the symmetrical VG1-C2, 0.16 mmol of both NHS and DCC were used due to the presence of two carboxyl groups. Reactions were monitored by mass spectrometry until complete conversion and then the product was separated through dilution in diethyl ether and filtration to obtain products as powders.

Squaraine-silane derivatives were then prepared by adding 3-aminopropyltriethoxysilane (APTS; 46.0 μ mol, 10 μ L for VG0-NHS and SO₃H-SQ-NHS; 92.0 μ mol, 20 μ L for VG1-C2-NHS) to squaraine-NHS solutions in 0.5 ml of anhydrous DMF and stirring the mixture for 24h at room temperature; reactions were monitored by thin layer chromatography until complete disappearance of former NHS esters. The obtained squaraine-silane derivatives (hereafter X-APTS, where X is the squaraine code) were then used without further purification in order to avoid the occurrence of self-polymerization.

Schemes of the syntheses are shown in the Supporting Information (hereafter SI).

2.1.3 Synthesis of squaraine-loaded silica NPs

Hybrid squaraine-silica NPs were prepared by the reverse microemulsion technique already reported in previous works[18,19,21]. Briefly, a water in oil microemulsion was prepared by mixing cyclohexane (75.0 ml), Triton X-100 (18.85 g), *n*-hexanol (18.0 ml) and distilled water (5.4 ml); the mixture was gently stirred for ca. 30 minutes and then 0.05 ml of a 0.01 M squaraine-APTS in DMF was added; after further 15 minutes, TEOS (1.0 ml, 4.5 mmol) and NH₄OH (28-30%, 0.7 ml) were added to start the NPs formation. Reaction was stirred for 16 hours at room temperature and then was stopped by adding 50.0 ml of acetone; particles were extracted from the supernatant by centrifugation (10k rpm, r.t.) and washed twice in ethanol and several times in distilled water by resuspension and centrifugation cycles until complete removal of the surfactant. Finally, squaraine-loaded silica NPs (hereafter X-NPs, where X is the squaraine code) were stored as suspensions in distilled water at room temperature in the dark until needed.

In order to attain possible optimization of the preparation technique, in two cases the hybrid NPs

172 preparation protocol was changed (*vide infra*) and the resulting materials were labeled as X-NPs-B.
173 For solvatochromic experiments, NPs stored as water suspensions were first centrifuged at 10k rpm
174 for 20 minutes and then resuspended using acetone. Then, NPs were washed twice by
175 centrifugation/resuspension cycles in order to completely remove water and, finally, the
176 concentration of the final suspensions was adjusted to 1 mg·ml⁻¹.

177

178 **2.2 Methods**

179

180 **2.2.1 Characterization of dyes**

181 Thin-layer chromatography was performed on silica gel 60 F254 plates. ESI-MS spectra were
182 recorded using a LCQ Thermo Advantage Max spectrometer, with electrospray interface and ion trap
183 as mass analyzer. The flow injection effluent was delivered into the ion source using nitrogen as
184 sheath and auxiliary gas. ¹H NMR (200 MHz) spectra were recorded on a Bruker Avance 200 NMR.

185

186 **2.2.2 UV-Vis absorption spectroscopy**

187 UV-VIS electronic absorption spectra of the squaraine in solution and of the supernatants derived
188 from nanoparticle extraction from the microemulsion mixture were measured by a Cary 300 Bio
189 spectrophotometer (Varian, Santa Clara, CA, USA), using quartz cuvettes (1 cm pathway length).

190 For the determination of absorption coefficients, every dye was weighed, (7.0-10.0 mg), and diluted
191 to 10.0 ml in a flask using DMSO. From this solution, 0.25 ml were taken and diluted to 25.0 ml with
192 the proper solvent (mother solution). Three dilutions were prepared by diluting 1.0, 2.5 and 5.0 ml of
193 this solution to 25.0 ml. Those solutions were analyzed by UV-Vis spectroscopy. Absorbance at the
194 λ_{max} for every diluted solution was plotted vs. dye concentration and a linear fitting was performed.
195 The slope of the plot is the molar absorption coefficient (ϵ). The determination was made, in duplicate,
196 by preparing two separate concentrated dye mother solutions in DMSO. The log ϵ obtained from the
197 two separate data sets was compared: if their difference was less or equal to 0.02 respect to their

198 average, the data were considered acceptable and the average of the two values was taken as the
199 official value. Otherwise, a further concentrated dye mother solution in DMSO was prepared, the
200 whole procedure was repeated and the log_e data were compared.

201

202 **2.2.3 UV-Vis photoemission spectroscopy**

203 Photoluminescence and excitation spectra in steady state mode were acquired using a Horiba Jobin
204 Yvon Fluorolog 3 TCSPC fluorimeter equipped with a 450-W Xenon lamp and a Hamamatsu R928
205 photomultiplier.

206 The absolute quantum yield of each dye in solution was determined combining Quanta-φ with
207 Fluorolog 3. The reported values are the average of three measurements using three different dye
208 solutions.

209 Fluorescence lifetimes were measured by the time correlated single photon counting method (Horiba
210 Jobin Yvon) using a 560 nm Horiba Jobin Yvon NanoLED as excitation source and an impulse
211 repetition frequency of 1 MHz positioned at 90° with respect to a TBX-04 detector. Lifetimes were
212 calculated using DAS6 decay analysis software.

213

214 **2.2.4. High resolution transmission electron microscopy (HRTEM)**

215 Size and morphology of NPs were analyzed with a 3010 Jeol microscope operating at 300 kV. A
216 droplet of each nanoparticle water suspension (1.0 mg ml⁻¹) was spread on a copper grid coated with
217 a carbon film and then water was allowed to slowly evaporate in order to limit particle agglomeration.
218 Size distribution was evaluated by measuring at least 300 nanoparticles and the mean diameters were
219 calculated as $d_m = \sum d_i n_i / \sum n_i$ (n_i = number of particles of diameter d_i); results were reported as $d_m \pm$
220 stdv.

221

222

223

224 3. Results and discussion

225

226 3.1 Synthesis of squaraines and squaraine-silane derivatives

227 VG0 and VG1-C2 squaraines were prepared via a microwave condensation reaction based on a
228 previously reported procedure[3] while SO₃H-SQ was synthesized by a microwave-assisted
229 condensation of 5-sulfo-indolenine salt **1**[20] and carboxyemisquarate **2**[3] (see Scheme 1).

230 Squaraine-silane derivatives were prepared via a previously reported method [12] through the NHS
231 ester modification of the squaraine carboxylic group and subsequent reaction with APTS (see Scheme
232 S2 in the SI for SO₃H-SQ modification).

233

234 3.2 Photophysical properties of squaraines in solution

235 The photophysical behaviour of each squaraine dye in solution was investigated together with the
236 determination of the correspondent molar decadic absorption coefficient and absolute quantum yield
237 by means of absorption and both steady-state and time-resolved photoemission spectroscopies (see
238 Table 1).

239 The UV-Vis absorption spectra (see Figure 2) of the squaraine dyes show absorption maxima between
240 630 nm and 646 nm with high molar extinction coefficients (log ϵ around 5.40 in organic solvents and
241 4.51 in water). The main absorption peak is associated to the $\pi \rightarrow \pi^*$ HOMO–LUMO transitions,
242 mainly localized on the squarainic core[22,23], while the shoulder at higher energy is due to the
243 HOMO-LUMO+1 transition. When excited within the absorption band at room temperature, the three
244 types of squaraines emit a luminescence spectrum almost specular to the absorption one, with maxima
245 ranging from 639 to 656 nm, thus with small Stokes shifts as expected for squaraine dyes[24].

246

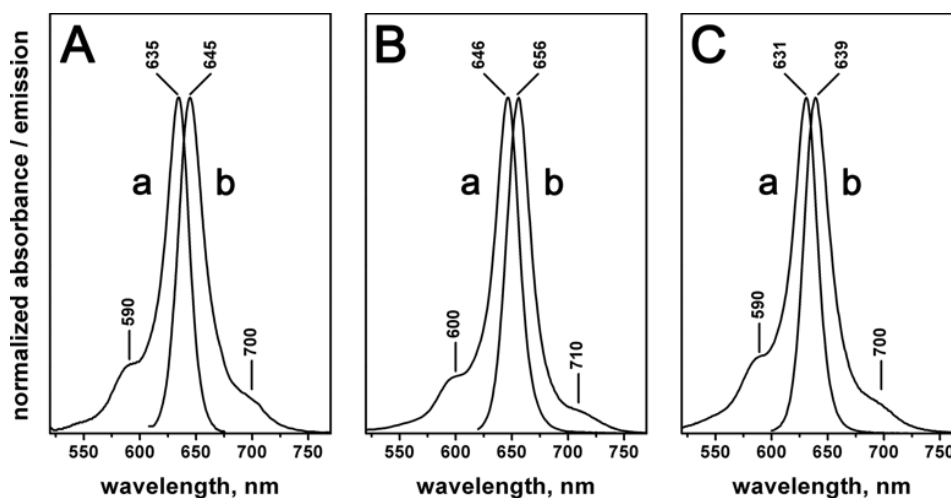


Figure 2. Absorption (a) and emission spectra ($\lambda_{\text{ex}} = 590$ nm) (b) of **VG0** in methanol (panel A), **VG1-C2** in acetone (panel B) and **SO₃H-SQ** in water (panel C).

Fluorescence lifetime and quantum yield of VG0 in methanol and VG2-C1 in acetone are in the ranges typical for squaraines in organic media [25]. Also the much lower τ and Φ of SO₃H-SQ is in agreement with the expected photoemission behaviour in water [26,27].

Table 1. Main optical characteristics of **VG0** in methanol, **VG1-C2** in acetone and **SO₃H-SQ** in water.

	λ_{abs} (nm)	$\log \epsilon$	λ_{em} (nm)	τ (ns)	ϕ
VG0 [†]	635	5.39	645	0.28 (100%)	0.15
VG1-C2 [*]	646	5.40	656	0.99 (100%)	0.27
SO₃H-SQ [□]	631	4.51	639	0.11 (100%)	0.023

[†] in methanol, ^{*} in acetone, [□] in water

3.3 Shape, size and dye-content of squaraine loaded silica NPs

Representative TEM micrographs of the three squaraine-NPs samples are shown in figure 3, where the highly regular spherical shape (upper panels) and quite homogeneous size of NPs around a mean diameter of 50 nm (lower panels) can be appreciated. Hence, on the basis of the TEOS-to-SiO₂ conversion yield, the density of NPs (ca. 2.2 g·cm⁻³)[19] and the calculated average nanoparticle volume, the total number of NPs obtained by each preparation was estimated.

As a second step, for each sample the total amount of squaraine molecules associated to NPs was calculated as the difference between their initial amount and that remained in the reaction media after the accomplishment of the formation of NPs, as determined spectrophotometrically after the separation of NPs by centrifugation. This was possible because no squaraine degradation products were detected in the UV-Vis spectra of the post-reaction liquid medium. Thus, the average number of dye molecules per nanoparticle was calculated (Table 2). Apparently, the VG0-APTS adduct was unable to participate to the formation of NPs, whereas this was the case for ca. 45 % and 65% of VG1-C2-APTS and SO₃H-SQ-APTS species present in the relevant reaction media, resulting in ca. 50 and 70 dye molecules-per-NP, respectively.

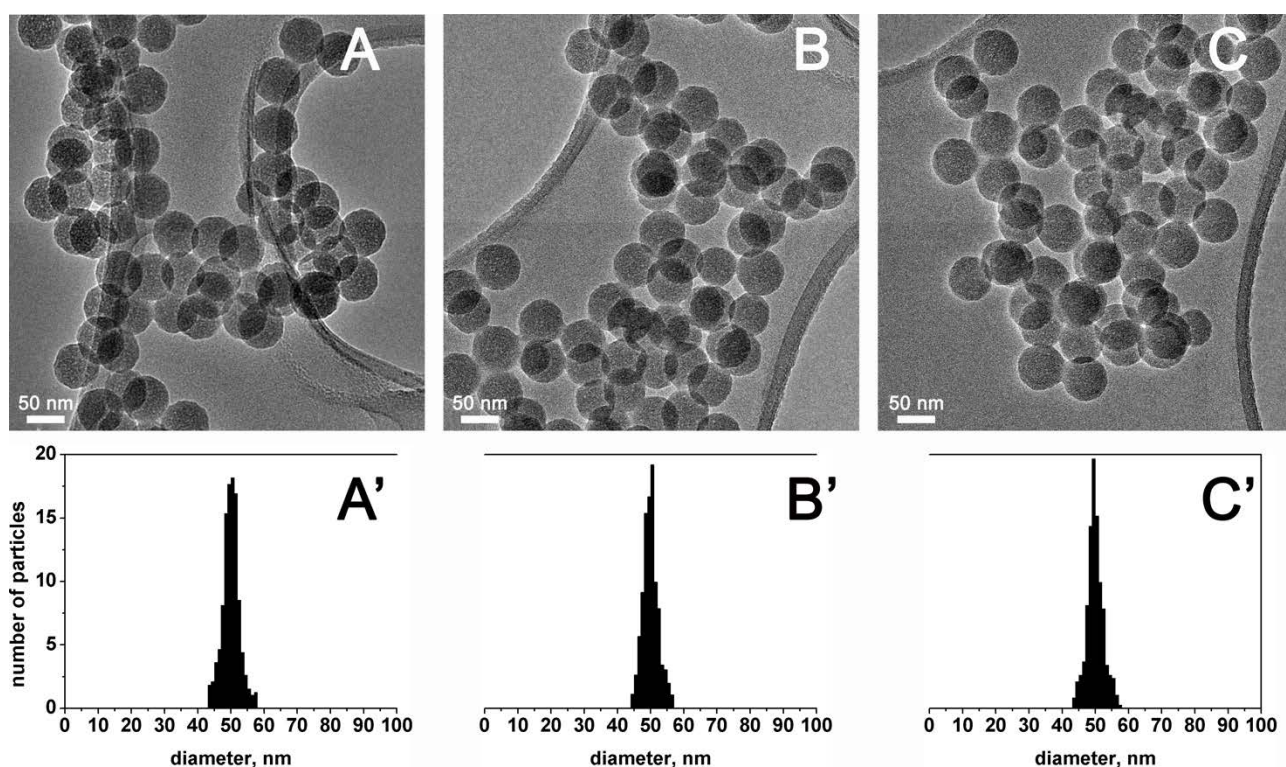


Figure 3. Representative TEM images of VG0-NPs (A), VG1-C2-NPs (B) and SO₃H-SQ-NPs (C) and correspondent size distribution histograms. Original magnification of images: 500000 \times . Scale bar: 50 nm

Table 2. Yields of entrapment of squaraine-APTS molecules in silica NPs

	Yield of Squaraine-APTS molecules entrapment (%)	Squaraine- APTS molecules per NP (n°)
VG0-NPs	0	0
VG1-C2-NPs	46	47
SO₃H-SQ-NPs	66	68
VG1-C2-NPs-B	41	42
SO₃H-SQ-NPs-B	63	65

The lack of encapsulation of VG0-APTS in the silica matrix should be rationalized in terms of a so poor hydrophilicity of this squaraine derivative to prevent its transfer into the water pool in the core of reverse micelles, and thus this squaraine derivative will be no longer considered. Conversely, the presence of two triethoxysilane moieties in VG1-C2-APTS counterbalance enough the hydrophobicity of the squaraine motif to allow this derivative to reach the water pools and participate to hydrolysis and condensation with TEOS during the formation of NPs. As expected, a stronger effect resulted from the presence of the sulphonic group in SO₃H-SQ-APTS, which was involved in the formation of NPs in a larger extent. However, the rate of transfer into the micelles of neither VG1-C2-APTS nor SO₃H-SQ-APTS was high enough to allow all the dye derivative to participate to the reaction before the accomplishment of the formation of the NPs.

3.4 Photoemission properties and location of the entrapped squaraines

In order to evaluate any possible modification of the photophysical behaviour of the entrapped fluorophores, steady state photoemission and excitation spectra of hybrid VG1-C2-NPs and SO₃H-SQ-NPs were recorded in suspension and compared to the data obtained for the correspondent dye derivatives in solution (figure 4). Data obtained for VG1-C2 and VG1-C2-APTS were similar, indicating that the derivatization did not modify significantly the photophysical behaviour of the dye.

301 $\text{SO}_3\text{H-SQ}$ was only soluble in water, and this prevented a comparison with $\text{SO}_3\text{H-SQ-APTS}$ in the
302 same medium, because of the sensitivity of the derivative to hydrolysis. Thus, the pristine VG1-C2
303 and $\text{SO}_3\text{H-SQ}$ were considered for the comparisons with their derivative associated to NPs.
304 For both types of hybrid NPs, excitation instead of absorption in transmission was recorded because
305 the lower sensitivity of the latter did not allow to record spectra with an acceptable signal-to-noise
306 ratio at suspension concentrations low enough to avoid light scattering.
307 In figure 4 panel A, excitation and photoemission spectra of VG1-C2 in solution and VG1-C2-NPs
308 in suspension are reported; acetone was used as solution and suspension medium due to the low
309 solubility of VG1-C2 in water. It can be clearly observed that both excitation and emission signals of
310 the NPs are identical to the correspondent ones of the fluorophore in solution suggesting that no
311 modifications of the energies and probabilities of the electronic transitions occurred due to the
312 association with the inorganic matrix. On the contrary, in the case of $\text{SO}_3\text{H-SQ}$ (figure 4, panel B),

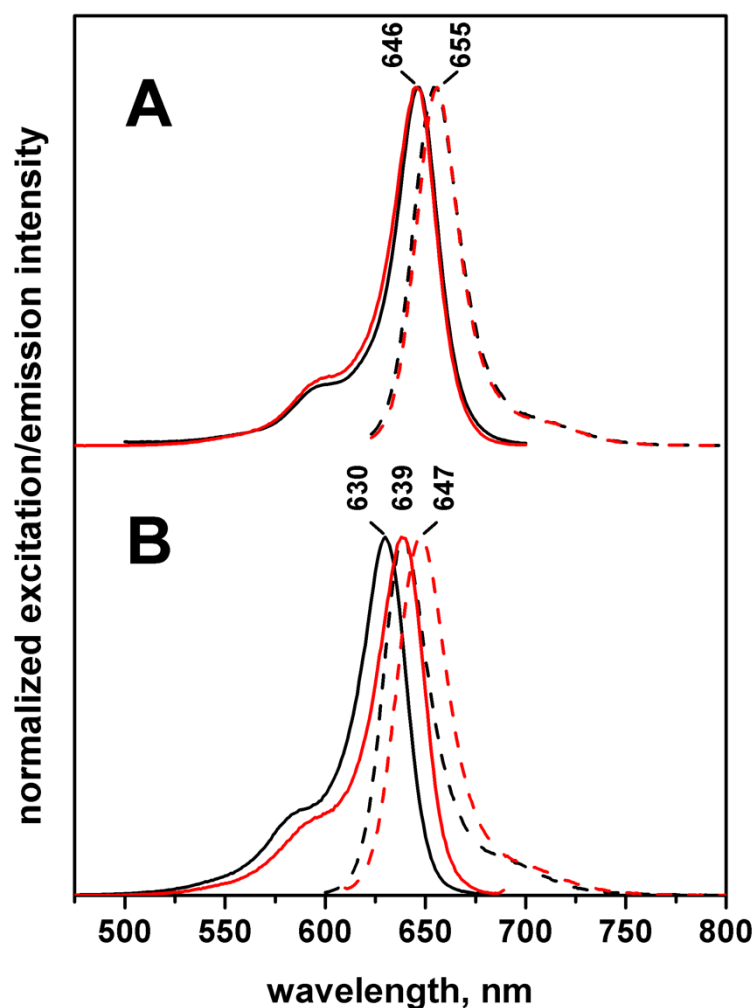


Figure 4. Panel A: excitation (solid curves, $\lambda_{em} = 655$ nm) and photoemission (dashed curves, $\lambda_{exc} = 590$ nm) spectra of VG1-C2 in acetone solution (black curve, $5.0 \cdot 10^{-6}$ M) and VG1-C2-NPs in acetone suspension (red curve, $3.0 \cdot 10^{-8}$ mg·ml⁻¹); Panel B: excitation (solid curves, $\lambda_{em} = 640$ nm) and photoemission (dashed curves, $\lambda_{exc} = 590$ nm) spectra of SO₃H-SQ in water solution (black curve, $5.0 \cdot 10^{-6}$ M) and SO₃H-SQ-NPs in water suspension (red curve, $3.0 \cdot 10^{-8}$ mg·ml⁻¹). All spectra were normalized with respect to the maximum for the sake of clarity.

where the hydrophilicity of the dye allowed to use water as medium for both the molecule in solution and the hybrid NP suspension, the association of dye derivatives with silica produced a decrease of the energies of absorption and fluorescence transitions as indicated by the 9 nm red shift of both signals. The coincidence of the shape of the spectra profiles exhibited by both dye/hybrid NPs pairs allowed to exclude the occurrence of intra-particle autoabsorption effects. Hence, as the framework of amorphous silica is apolar[28] the red-shift observed for SO₃H-SQ-NPs should be reasonably

assigned to a solvatochromic effect due to the decrease of the polarity of the environment experienced by entrapped squaraine derivatives with respect to the ones in water solution. The solvathocromic behavior of the SO₃H-SQ in solution were reported in figure S1 in the SI for the sake of comparison. Time-resolved photoemission measurements were also carried out, and the results are listed in table 3, compared with relevant cases of squaraine derivatives in solution. The targeted suspension medium for hybrid NPs is water, but also acetone was considered because of its lower polarity, thus useful to reveal possible solvatochromic effects due to dye molecules not entrapped in the bulk of NPs. For all suspensions of hybrid NPs, bi-functional equations were necessary to fit the decay curves, indicating that for both VG1-C2-APTS and SO₃H-SQ-APTS derivatives two different scenarios of interaction with the silica host are present. For VG1-C2-APTS, independently on the suspension medium, one fluorescence lifetime (τ^0_F) is slightly longer than what found for the molecular form in acetone solution, whereas the other (τ^1_F) appears increased of ca. 2.5 times with respect to that comparative form. In the case of SO₃H-SQ-APTS, the association with the silica matrix resulted in two lifetimes both significantly longer than for the molecular form in water solution, with an increase of ca. 7-10 and ca. 20 times, for τ^0_F and τ^1_F , respectively. For both types of hybrid dye-SiO₂ NPs, the relative population of fluorescent molecules showing the longer lifetime is the more abundant by far. For hybrid dye-NPs, the increase of fluorescence lifetime is the result of the decrease in rotational degrees of freedom, and in possible detrimental effects due to the interaction with highly polar media, such as water. Thus, data obtained for SO₃H-SQ-NPs indicate that SO₃H-SQ derivatives should be not simply anchored on the surface of NPs. Because of the similarity of τ^1_F values, significantly longer than the fluorescence lifetime of VG1-C2-APTS in acetone solution, the same should occur at least for the most abundant fraction of fluorescent dyes in VG1-C2-NPs. Conversely, the other fraction should experience an interaction with its environment with more limited differences with respect of acetone as solvent.

Noticeably, the time resolved photoemission behavior of both VG1-C2-NPs and SO₃H-SQ-NPs appeared sensitive to the suspension medium, with a slight increase of both τ^0_F and τ^1_F and, more significantly, with the transfer of ca. a 10% of fluorescent molecules between the relative abundances of dyes showing different fluorescence lifetime.

Table 3. Emission decay times ($\lambda_{exc} = 560$ nm) of: VG1-C2 in acetone solution ($5 \cdot 10^{-7}$ M); VG1-C2-NPs and VG1-C2-NPs-B in acetone and water suspension ($0.1 \text{ mg} \cdot \text{ml}^{-1}$); SO₃H-SQ in water solution ($1 \cdot 10^{-6}$ M); SO₃H-SQ-NPs and SO₃H-SQ-NPs-B in water and acetone suspension ($0.1 \text{ mg} \cdot \text{ml}^{-1}$)

	Medium	τ^0_F (ns)	% τ^0_F (ns)	τ^1_F (ns)	% τ^1_F (ns)	χ^2
VG1-C2	acetone	0.99	100	---	---	1.01
VG1-C2-NPs	acetone	1.19	21	2.42	79	1.12
	water	1.06	31	2.37	69	1.04
SO₃H-SQ-NPs	acetone	1.10	15	2.38	85	1.08
	water	0.80	21	2.31	79	1.02
SO₃H-SQ	water	0.11	100	---	---	1.03
VG1-C2-NPs-B	acetone	1.35	25	2.44	75	1.04
	water	1.02	43	2.19	57	1.13
SO₃H-SQ-NPs-B	acetone	1.21	35	2.62	65	1.07
	water	0.99	46	2.38	54	1.02

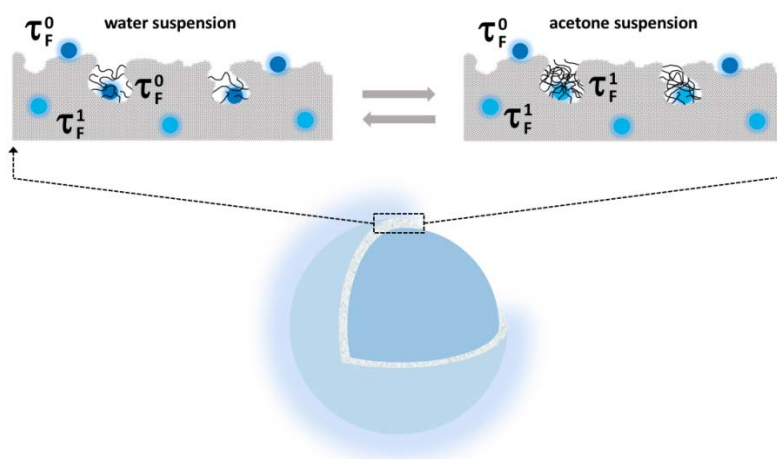
For both VG1-C2-NPs and SO₃H-SQ-NPs, fluorescent dyes showing the longer lifetime are candidate to be depicted as well entrapped in the silica matrix; however, their sensitivity to the suspension medium, and in particular their change in relative abundance, pose a problem.

In this respect, it is useful to remind that silica NPs prepared by the microemulsion or Stöber methods are characterized by the presence of domains, extended from the surface towards the interior, of non-completely condensed silica, resulting in a mass fractal structure sensitive to changes in the external environment [29,30]. Moreover, H/D isotopic exchange indicated that such domains can be infiltrated by water molecules[21]. Therefore, although the sensitivity of the measurement technique

369 did not allow to distinguish more than two relative abundances of fluorescent dyes for each type of
 370 hybrid NPs, the obtained data could be explained by assuming the presence of three ensembles of
 371 fluorescent dyes in the NPs (scheme 2):

- 372 i) a most abundant fraction, characterized by the longer fluorescent lifetime, τ_F^1 (ca. 70% and 80%
 373 for VG1-C2-NPs and SO₃H-SQ-NPs, respectively), well constrained by the silica matrix, likely
 374 in its fully condensed part, insensitive to changes in suspension medium
- 375 ii) a fraction of ca. 20% for VG1-C2-NPs and 15% for SO₃H-SQ-NP, showing the shorter
 376 fluorescent lifetime τ_F^0 , located at/near the nanoparticle surface and less constrained by the silica
 377 matrix independently on the type of suspension medium
- 378 iii) a fraction, ca. 10% and 6% for VG1-C2-NPs and SO₃H-SQ-NPs, respectively, located in not
 379 fully condensed parts of silica matrix more sensitive to the nature of the suspension medium,
 380 where fluorescent dyes are less constrained when these parts are infiltrated by water.

381



382

383 **Scheme 2.** Distribution of dye molecules in the NPs explaining the different sensitivity to the
 384 suspension medium

385

386

387

388

389 **3.5 Dyes in solution vs hybrid NPs: comparison of fluorescence intensity**

390 Because of the direct proportionality between fluorescence lifetime and quantum yield[31], the
391 measured increase of fluorescence lifetime for all dye fractions in SO₃H-SQ-NPs and the most
392 abundant one for VG1-C2-NPs appears the basis for expecting an increase in fluorescence intensity
393 of hybrid NPs suspensions with respect to the squaraine derivatives in solutions, for equivalent dye
394 molar concentrations. Hence, the following experimental procedure was used for VG1-C2 and
395 SO₃H-SQ-based systems, differing only for the suspension medium, as described in the previous
396 section. On the basis of the calculated number of squaraine per nanoparticle (table 2), a series of
397 suspensions at known dye concentration was prepared for both VG1-C2-NPs and SO₃H-SQ-NPs, as
398 well as a series of solutions of VG1-C2 and SO₃H-SQ in the same concentration range. The
399 photoemission spectra were recorded, strictly using the same excitation conditions, and the integrated
400 intensities of photoemission spectra were plotted with respect to the correspondent concentration
401 values (figure 5). A straight linear dependence was obtained, clearly indicating that the measurements
402 were affected by neither light scattering nor inter-particle auto-absorption effects.

403

404

405

406

407 *Part of the page left intentionally blank,*

408 *in order to show Figure 5 and the related caption in the same page*

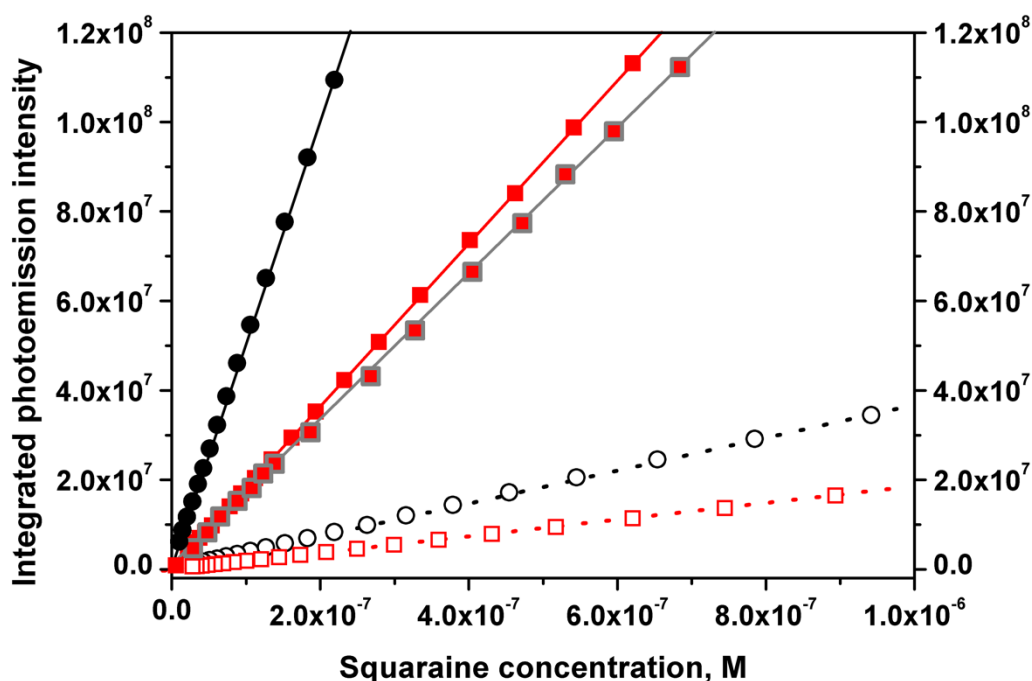
409

410

411

412

413



414

415 **Figure 5.** Comparison of the integrated intensities of photoemission spectra ($\lambda_{\text{exc}} = 590$ nm) of
 416 VG1-C2 in acetone solution (black solid dots), VG1-C2-NPs in acetone and water suspension (red
 417 solid squares and grey bordered red squares, respectively), SO₃H-SQ in water solution (black empty
 418 dots) and SO₃H-SQ-NPs in water suspension (red empty squares)

419

420 In agreement with the absolute quantum yields (table 1), solutions of the two squaraines produces
 421 significantly different fluorescence outputs, with VG1-C2 (black solid dots) showing integrated
 422 intensities of photoemission spectra ca. 13 times higher than SO₃H-SQ (black empty dots).
 423 Conversely, data obtained for the hybrid NPs were not in agreement with expectations: the integrated
 424 intensities of photoemission spectra of VG1-C2-NPs in both acetone (red solid squares) and water
 425 (grey bordered red squares) suspensions are ca. 35% and 30%, respectively, of what obtained for
 426 VG1-C2 solutions (black solid dots), and the relative decrease is limited to ca. 50% when comparing
 427 the SO₃H-SQ-NPs/SO₃H-SQ pair (red empty squares and black empty dots, respectively).

428 Such lower than expected fluorescence intensity should be due to a decrease of the decadic absorption
 429 coefficient of squaraines and/or a quenching of a part of them when linked to/entrapped in the silica

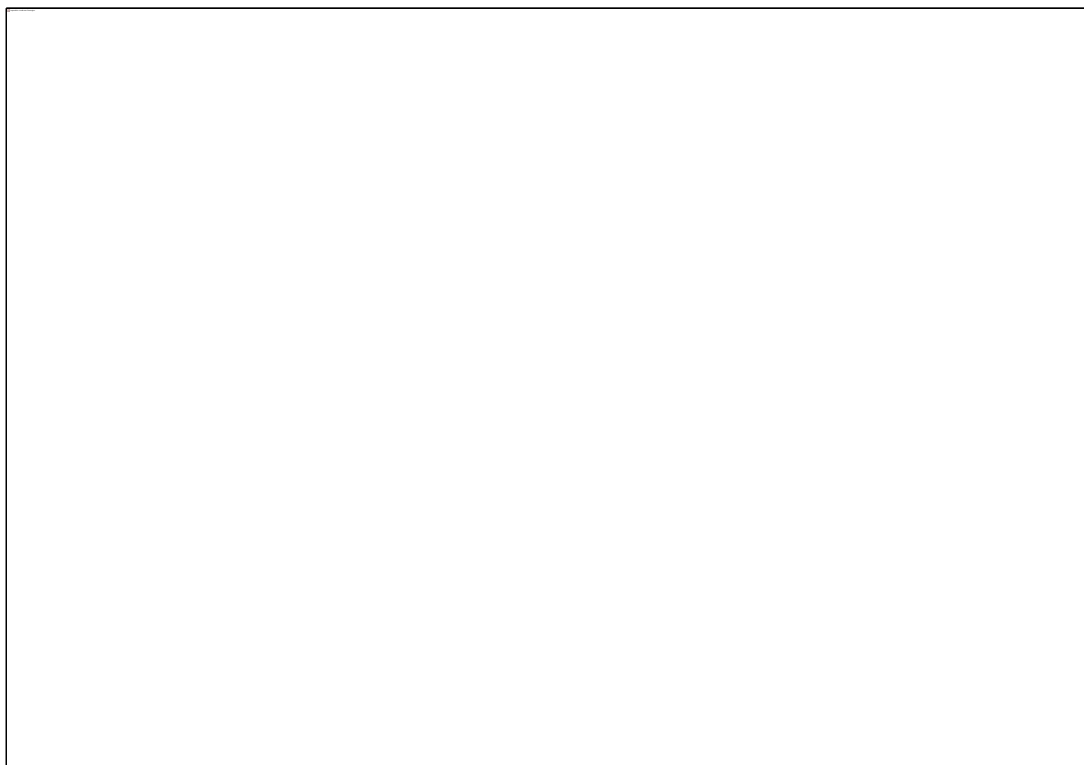
430 matrix. Non-light-scattering suspensions of hybrid NPs were too diluted to allow the recording of
431 absorbance spectra, and then no insights were obtained for the first possibility.

432 Focusing on fluorescence quenching, if occurred it might be of the concentration type, resulting from
433 the formation of aggregates of squaraine derivatives when involved in the growth of NPs. In
434 particular, SO₃H-SQ-APTS, highly hydrophilic and then easily transferred from the oil phase to the
435 inner water pool of reverse micelles, could have formed aggregates in the first steps of the reaction,
436 whereas the contrary might have occurred for VG1-C2-APTS, definitely less hydrophilic and then
437 involved in the reaction when the nanoparticle formation was almost accomplished.

438 Based on these hypotheses, two additional samples were prepared by modifying the synthesis
439 procedure with an opposite target, depending on the squaraine derivative considered. Thus, to dilute
440 in time the entering of SO₃H-SQ-APTS in the micelles, it was dosed in the reaction medium in small
441 aliquots at regular time intervals (0.01 ml every 10 min) during the first hour of the NPs synthesis.
442 Conversely, VG1-C2-APTS was added to the microemulsion as solution in *n*-hexanol, i.e. the
443 co-surfactant of micelles, in order to facilitate its partition at the boundary between the oil and water
444 phases. In this way, the shortening of the diffusion path should allow this squaraine derivative to be
445 involved not only in late steps of the formation of NPs. These two samples were labeled as
446 SO₃H-SQ-NPs-B and VG1-C2-NPs-B.

447 As for the previous cases, the amount of dyes effectively associated with NPs was calculated, and
448 values very close to the ones already found for the previous corresponding hybrid NPs were obtained
449 (table 2). The same occurred for steady-state and time resolved photoemission data (Figure S2 in the
450 SI and table 3, respectively). Conversely, the integrated intensity of the photoemission spectra of dye
451 equimolar SO₃H-SQ solutions/hybrid NPs suspensions in water appear almost coincident, and the
452 values obtained for VG1-C2-NPs-B in acetone and water suspensions are ca. 90% and 70%,
453 respectively of those measured with VG1-C2 in acetone solutions (figure 6). Thus, the second set of
454 hybrid NPs shows a definitely better performance as photoemitters with respect to the first one (see
455 figure 5).

456 Apparently, the strategies adopted to affect the distribution of squaraine derivatives on/in the silica
457 NPs were successful, at least partly. In fact, if all dye molecules in hybrid NPs were fluorescent,
458 based on the measured increase in photoemission lifetime, the fluorescence intensity of their
459 suspensions should exceed that of equimolar dye solutions by far. A specific investigation in this
460 respect will be the object of a future investigation.



461
462 **Figure 6.** Comparison of the integrated photoemission intensities ($\lambda_{\text{exc}}=590$ nm) of VG1-C2 in
463 acetone solution (black solid dots), VG1-C2-NPs-B in acetone and water suspension (red solid
464 squares and grey bordered red squares, respectively), SO₃H-SQ in water solution (black empty dots)
465 and SO₃H-SQ-NPs-B in water suspension (red empty squares).
466

467

468

469

470

471

472

473 **4. Conclusion**

474

475 The preparation of hybrid squaraines-silica nanoparticles showing, in aqueous suspension, a
476 photoluminescence emission intensity per dye molecule equivalent to parent water insoluble
477 squaraine molecules, when in organic solution, has been achieved successfully. Such achievement
478 stems from the adopted molecular engineering approach, based on the hypothesis that the relative
479 hydrophobicity of dye-3-aminopropyltriethoxysilane (APTS) adducts and tetraethylorthosilicate
480 (TEOS) is a key parameter ruling the distribution of fluorophores within the nascent silica matrix
481 when the reverse microemulsion method is used for producing hybrid dye-SiO₂ nanoparticles. Such
482 hypothesis, developed in previous studies on the preparation of hybrid cyanine- SiO₂
483 nanoparticles[21], and recently assumed also by other researchers[32] has been here confirmed also
484 for squaraines, and in addition, the possibility to improve the tuning of the process by administering
485 the squaraine-APTS adduct with the co-surfactant has been demonstrated. This is the first report, at
486 the best of our knowledge, on molecular factors ruling the dispersion of squaraines in solid silica
487 nanoparticles, but the number of dye molecules per nanoparticles and likely their photoluminescent
488 fraction are significantly lower with respect what obtained with cyanine dyes [19, 21]. Thus, the
489 future steps of this research will be aimed to overcome this gap, targeting more bright hybrid
490 squaraine-SiO₂ nanoparticles.

491

492

493 **Acknowledgments**

494 This work was supported by the Fondazione Cassa di Risparmio di Torino, Italy (STemMRef project,
495 cod. ID 48853).

496

497

498

499 **References**

500

- 501 [1] Luo S, Zhang E, Su Y, Cheng T, Shi C. A review of NIR dyes in cancer targeting and
502 imaging. *Biomaterials* 2011;32:7127–38. Doi:10.1016/j.biomaterials.2011.06.024.
- 503 [2] Kim D, Lee N, Park Y Il, Hyeon T. Recent Advances in Inorganic Nanoparticle-Based NIR
504 Luminescence Imaging: Semiconductor Nanoparticles and Lanthanide Nanoparticles.
505 *Bioconjug. Chem.* 2017;28:115–23. Doi:10.1021/acs.bioconjchem.6b00654.
- 506 [3] Barbero N, Magistris C, Park J, Saccone D, Quagliotto P, Buscaino R, et al. Microwave-
507 assisted synthesis of near-infrared fluorescent indole-based squaraines. *Org. Lett.*
508 2015;17:3306–3309. Doi:10.1021/acs.orglett.5b01453
- 509 [4] Serpe L, Ellena S, Barbero N, Foglietta F, Prandini F, Gallo MP, et al. Squaraines bearing
510 halogenated moieties as anticancer photosensitizers: Synthesis, characterization and
511 biological evaluation. *Eur. J. Med. Chem.* 2016;113:187–97.
512 Doi:10.1016/j.ejmech.2016.02.035.
- 513 [5] Zollinger H. *Color Chemistry*. Second Ed. Weinheim: VCH; 1991.
- 514 [6] Karpenko IA, Klymchenko AS, Gioria S, Kreder R, Shulov I, Villa P, et al. Squaraine as a
515 bright, stable and environment- sensitive far-red label for receptor-specific cellular imaging
516 *Chem. Commun.* 2015;51:2960–3. Doi:10.1039/C4CC09113B.
- 517 [7] Arunkumar E, Fu N, Smith BD. Squaraine-Derived Rotaxanes : Highly Stable , Fluorescent
518 Near-IR Dyes. *Chem. - A Eur J.* 2006;12:4684–90. Doi:10.1002/chem.200501541.
- 519 [8] Sreejith S, Joseph J, Lin M, Menon NV, Borah P. Near-Infrared Squaraine Dye Encapsulated
520 Micelles for in Vivo Fluorescence and Photoacoustic Bimodal Imaging. *ACS Nano*
521 2015;9:5695–704. Doi:10.1021/acs.nano.5b02172.
- 522 [9] Wu F, Wang H. Nano-Con fi ned Squaraine Dye Assemblies: New Photoacoustic and Near-
523 Infrared Fluorescence Dual-Modular Imaging Probes in Vivo. *Bioconjug. Chem.*
524 2014;25:2021–2029. Doi:10.1021/bc5003983.

- 525 [10] Conterposito E, Benesperi I, Toson V, Saccone D, Barbero N, Palin L, et al. High-Throughput
526 Preparation of New Photoactive Nanocomposites. *ChemSusChem* 2016;9:1279–89.
527 Doi:10.1002/cssc.201600325.
- 528 [11] Miletto I, Fraccarollo A, Cossi M, Marchese L, Barbero N, Barolo C. Mesoporous silica
529 nanoparticles incorporating squaraine-based photosensitizers: a combined experimental and
530 computational approach. *Dalt. Trans.* 2018;15–8. Doi:10.1039/c7dt03735j.
- 531 [12] Sreejith S, Zhao Y. Graphene Oxide Wrapping on Squaraine-Loaded Mesoporous Silica
532 Nanoparticles for Bioimaging. *J. Am. Chem. Soc.* 2012;134:17346–17349.
533 Doi:10.1021/ja305352d.
- 534 [13] Santra S, Dutta D, Moudgil BM. Functional dye-doped silica nanoparticles for bioimaging,
535 diagnostics and therapeutics. *Food Bioprod. Process.* 2005;1988:136–40.
536 Doi:10.1205/fbp.04400.
- 537 [14] Accomasso L, Rocchietti EC, Raimondo S, Catalano F, Alberto G, Giannitti A, et al.
538 Fluorescent Silica Nanoparticles Improve Optical Imaging of Stem Cells Allowing Direct
539 Discrimination between Live and Early-Stage Apoptotic Cells. *Small* 2012;3192–200.
540 Doi:10.1002/sml.201200882.
- 541 [15] Liu C, Yu H, Li Q, Zhu C, Xia Y. Brighter, More Stable, and Less Toxic: A Host – Guest
542 Interaction- Aided Strategy for Fabricating Fluorescent Silica Nanoparticles and Applying
543 Them in Bioimaging and Biosensing at the Cellular Level. *ACS Appl. Mater. Interfaces*
544 2018;10:16291–8. Doi:10.1021/acsami.8b03034.
- 545 [16] Larson DR, Ow H, Vishwasrao HD, Heikal AA, Wiesner U, Webb WW, et al. Silica
546 Nanoparticle Architecture Determines Radiative Properties of Encapsulated Fluorophores
547 *Chem. Mater.* 2008;2677–84. Doi: 10.1021/cm7026866
- 548 [17] Arriagada FJ. Synthesis of Nanosize Silica in a Nonionic Water-in-Oil Microemulsion :
549 Effects of the Water / Surfactant Molar Ratio and Ammonia Concentration. *J. Colloid.*
550 *Interface Sci.* 1999;220:210–20. Doi: 10.1006/jcis.1998.5985

- 551 [18] Miletto I, Gilardino A, Zamburlin P, Dalmazzo S, Lovisolo D, Caputo G, et al. Highly bright
552 and photostable cyanine dye-doped silica nanoparticles for optical imaging: Photophysical
553 characterization and cell tests. *Dye Pigment* 2010;84:121–7.
554 Doi:10.1016/j.dyepig.2009.07.004.
- 555 [19] Alberto G, Miletto I, Viscardi G, Caputo G, Latterini L, Coluccia S, et al. Hybrid Cyanine -
556 Silica Nanoparticles : Homogeneous Photoemission Behavior of Entrapped Fluorophores and
557 Consequent High Brightness Enhancement. *J. Phys. Chem. C* 2009;113:21048–53. Doi:
558 10.1021/jp907415q
- 559 [20] Winstead AJ, Nyambura G, Matthews R, Toney D, Oyaghire S. Synthesis of quaternary
560 heterocyclic salts. *Molecules* 2013;18:14306–19. doi:10.3390/molecules181114306.
- 561 [21] Alberto G, Caputo G, Viscardi G, Coluccia S, Martra G. Molecular Engineering of Hybrid
562 Dye – Silica Fluorescent Nanoparticles: Influence of the Dye Structure on the Distribution
563 of Fluorophores and Consequent Photoemission Brightness. *Chem. Mater.*
564 2012;24:2792–2801. doi:10.1021/cm301308g.
- 565 [22] Yum J-H, Walter P, Huber S, Rentsch D, Geiger T, Nüesch F, et al. Efficient far red
566 sensitization of nanocrystalline TiO₂ films by an unsymmetrical squaraine dye. *J. Am.*
567 *Chem. Soc.* 2007;129:10320–1. doi:10.1021/ja0731470.
- 568 [23] Park J, Barbero N, Yoon J, Dell’Orto E, Galliano S, Borrelli R, et al. Panchromatic
569 symmetrical squaraines: a step forward in the molecular engineering of low cost blue-
570 greenish sensitizers for dye-sensitized solar cells. *Phys. Chem. Chem. Phys.* 2014;16:24173–
571 7. doi:10.1039/C4CP04345F.
- 572 [24] Borrelli R, Ellena S, Barolo C. Theoretical and experimental determination of the absorption
573 and emission spectra of a prototypical indolenine-based squaraine dye. *Phys. Chem. Chem.*
574 *Phys.* 2014;16:2390–8. doi:10.1039/c3cp54298j.
- 575 [25] Park J, Barolo C, Sauvage F, Barbero N, Benzi C, Quagliotto P, et al. Symmetric vs.
576 asymmetric squaraines as photosensitisers in mesoscopic injection solar cells: a structure–

- property relationship study. Chem. Commun. 2012;48:2782. doi:10.1039/c2cc17187b.
- [26] Tatarets AL, Fedyunyayeva IA, Dyubko TS, Povrozin YA, Doroshenko AO, Terpetschnig EA, et al. Synthesis of water-soluble, ring-substituted squaraine dyes and their evaluation as fluorescent probes and labels. Anal. Chim. Acta 2006;570:214–23. doi:10.1016/j.aca.2006.04.019.
- [27] Markova LI, Terpetschnig EA, Patsenker LD. Comparison of a series of hydrophilic squaraine and cyanine dyes for use as biological labels. Dye Pigment 2013;99:561–70. doi:10.1016/j.dyepig.2013.06.022.
- [28] Legrand AP. The surface properties of silicas. New York: John Wiley; 1998.
- [29] Szekeres M, Tóth J, Dékány I. Specific Surface Area of Stoeber Silica Determined by Various Experimental Methods. Langmuir 2002;18:2678–85. doi:10.1021/la011370j.
- [30] Catalano F, Alberto G, Ivanchenko P, Dovbeshko G, Martra G. Effect of Silica Surface Properties on the Formation of Multilayer or Submonolayer Protein Hard Corona: Albumin Adsorption on Pyrolytic and Colloidal SiO₂ Nanoparticles. J. Phys. Chem. C. 2015;119:26493–26505. doi:10.1021/acs.jpcc.5b07764.
- [31] Lakowicz JR. Principles of Fluorescence Spectroscopy. Third Ed. Singapore: Springer; 2006.
- [32] Kabanov V, Press DJ., Huynh RPS, Shimizu GKH, Heyne B. Assessment of encapsulated dyes' distribution in silica nanoparticles and their ability to release useful singlet oxygen, Chem. Commun. 2018; 54; 6320–3. Doi:10.1039/c8cc03413c